

High Power Nanocomposite TiS_2 Cathodes for All-Solid-State Lithium Batteries

To cite this article: James E. Trevey *et al* 2011 *J. Electrochem. Soc.* **158** A1282

View the [article online](#) for updates and enhancements.

You may also like

- [A stable solid-state lithium–oxygen battery enabled by heterogeneous silicon-based interface](#)
Zhiqian Yu, Sheng Wang, Ting Zhu *et al.*
- [Li₃InCl₆-Coated High-Voltage Cathodes for Thiophosphate-Based Solid-State Li Batteries](#)
Feng Jin, Laras Fadillah, Mir Mehraj Ud Din *et al.*
- [High-Temperature Performance of All-Solid-State Lithium-Metal Batteries Having Li/Li₃PS₄ Interfaces Modified with Au Thin Films](#)
Atsutaka Kato, Motoshi Suyama, Chie Hotehama *et al.*



Your Lab in a Box!

The PAT-Tester-i-16: All you need for Battery Material Testing.

- ✓ All-in-One Solution with integrated Temperature Chamber!
- ✓ Cableless Connection for Battery Test Cells!
- ✓ Fully featured Multichannel Potentiostat / Galvanostat / EIS!

www.el-cell.com +49 40 79012-734 sales@el-cell.com


electrochemical test equipment





High Power Nanocomposite TiS₂ Cathodes for All-Solid-State Lithium Batteries

James E. Trevey, Conrad R. Stoldt,* and Se-Hee Lee**^z

Department of Mechanical Engineering, University of Colorado-Boulder, Boulder, Colorado 80309, USA

To deploy solid-state Li batteries in next-generation vehicles, it is essential to develop electrodes with durability, high energy and high power. Here we report on nanostructured composite cathode materials that enable solid-state Li batteries to cycle with durable high energy and high rate performance. Particle size of TiS₂ is reduced by planetary ball-milling to enhance performance of nanocomposite cathodes in solid-state Li batteries. The better utilization of active material and fast kinetics resulting from the size reduction of TiS₂ allow for highly reversible capacity in both room temperature and elevated temperature batteries. High power all-solid-state batteries have been constructed with nano-sized TiS₂ and demonstrated high power density over 1000 W kg⁻¹ for over 50 cycles, with a maximum power density of ~ 1400 W kg⁻¹. Galvanostatic intermittent titration technique and electrochemical impedance spectroscopy are employed in order to explain the extremely high rate capability of nanostructured TiS₂ nanocomposite.
© 2011 The Electrochemical Society. [DOI: 10.1149/2.017112jes] All rights reserved.

Manuscript submitted July 6, 2011; revised manuscript received August 23, 2011. Published November 1, 2011.

Lithium-ion batteries have the highest energy density of all commercialized rechargeable batteries.¹⁻³ In order to employ Li-ion batteries (LIBs) in next generation electric vehicles (HEVs and PHEVs), LIBs must satisfy many requirements: electrodes with long lifetimes, stability over a wide temperature range, high energy density, and high rate capability.⁴⁻⁸ However, large scale utilization of lithium-ion battery technology has been limited due to safety issues associated with liquid electrolytes and the low specific capacity of typical positive electrode materials such as LiCoO₂ (~140 mAh g⁻¹).^{3,9,10}

Liquid-containing rechargeable lithium-ion batteries have exhibited major safety issues in the past owing to the hazardous and flammable nature of commercialized liquid electrolytes.¹¹⁻¹³ Furthermore, liquid electrolyte decomposition with the electrode material has been shown to significantly decrease battery performance.^{14,15} Use of a nonflammable solid electrolyte in lithium-ion batteries offers the possibility of avoiding the safety issues associated with conventional lithium-ion batteries containing combustible liquid electrolytes.¹⁶⁻¹⁸ Simply, construction of an all-solid-state rechargeable lithium battery using solid electrolyte inherently resolves a large majority of the safety issues associated with lithium battery technology.¹⁹ Unfortunately, all-solid-state lithium batteries typically exhibit lower power density, which is attributed to the solid electrolyte, in regard to the low ionic conductivity, and the positive electrode, in regard to large interfacial resistances, poor kinetics, and undesired reactions with the solid electrolyte.^{18,20-23}

Despite its high cost and limited capacity, lithium cobalt oxide (LiCoO₂) is widely accepted as a positive electrode material for rechargeable lithium-ion batteries due to its high energy/power density capabilities.²⁴ Its capacity for highly reversible intercalation of lithium as well as long cycle life have proven LiCoO₂ highly suited for use in liquid-based rechargeable lithium-ion batteries.^{25,26} However, implementation of LiCoO₂ into all-solid-state batteries has resulted in high interfacial resistances between the electrode and electrolyte as a result of incompatibility of LiCoO₂ with solid electrolytes relating to the high oxidation potential of the oxide-based electrode materials.²⁰ This large interfacial resistance not only leads to poor reversibility and cycle life, but prevents all-solid-state rechargeable lithium-ion batteries from performing at high rates.^{27,28} Characteristically, a more effective cathode material for solid state integration would have an oxidation potential close to that of the electrolyte in order to prevent the formation of a highly resistive interface. Other popular positive electrode materials such as LiMn₂O₄ and LiNiCoO₂ have been explored in solid state but typically lead to similar behavior to that of LiCoO₂ with low reversible capacity, low power, and rapid capacity fade.^{11,29}

Titanium disulfide (TiS₂) is a well-known electrode material that exhibits high energy density and high power in lithium batteries.^{15,30} Since its inception as a prospective intercalation compound in the 1970's, its physical and electrochemical properties have been studied extensively.³¹ At the time, TiS₂ was considered the most promising electrode material because it possesses exceedingly high conductivity and lithium diffusion rates, as well as being the lightest and cheapest of all group IVB and VB layered dichalcogenides.³² Whittingham et. al. performed considerable research on TiS₂ as an electrode material for lithium batteries and revealed it to be a very stable and high capacity electrode material that exhibits long cycle life.³³ However, while TiS₂ performed exceptionally well as a cathode material, it required a lithium battery construction that was not viable due to safety problems with Li dendrite formation in liquid electrolytes.⁹ TiS₂ was later shown to be compatible in a thin-film solid state construction but was never fully explored in an all-solid-state bulk-type construction. The introduction of layered oxides by Goodenough et al., lithium-ion "rocking chair" batteries by Murphy et al. and Scrosati et al., and development of the first lithium-ion batteries by Sony in the 1990's deterred further exploration of TiS₂ lithium batteries.⁹

In this work we demonstrate TiS₂ as a suitable cathode material for construction of all-solid-state lithium batteries. The fast kinetic and conductive properties, as well as moderate electrode potential, enable its successful use in solid state batteries. As proposed by Whittingham et al., we demonstrate that no conductive additive is required in constructing the composite cathode, as the electronic conductivity of TiS₂ is sufficiently high for fast electron transport through the composite electrode to the current collector.^{25,30} We reduce particle size of TiS₂ as a way to effectively increase utilization of active materials and improve the power density.⁸

Results and Discussion

Nanostructured Materials Characterization.— In recent years, high energy ball milling has been shown to be a very effective means of particle size reduction.³⁴ In addition, it is a room temperature process that is relatively fast and low cost.³⁵ The high energy attrition process involves grinding between two surfaces, the ball and the inner surface of containing jar, that results in particle breakage. It has been shown that smaller ball size will maintain a smaller contact area for grinding and result in reduced particle size.³⁴ In this respect, we used different size balls during ball milling to achieve a range of sizes for materials.

Field emission scanning electron microscope (FESEM) images of the various sizes of TiS₂ materials are shown in Figure 1. As-received TiS₂ with no ball-milling modification has been classified in this work as non-ball-milled TiS₂ (NBM) for simplicity. NBM exhibits a very large particle size distribution and an average particle size of

* Electrochemical Society Active Member.

^z E-mail: sehee.lee@colorado.edu

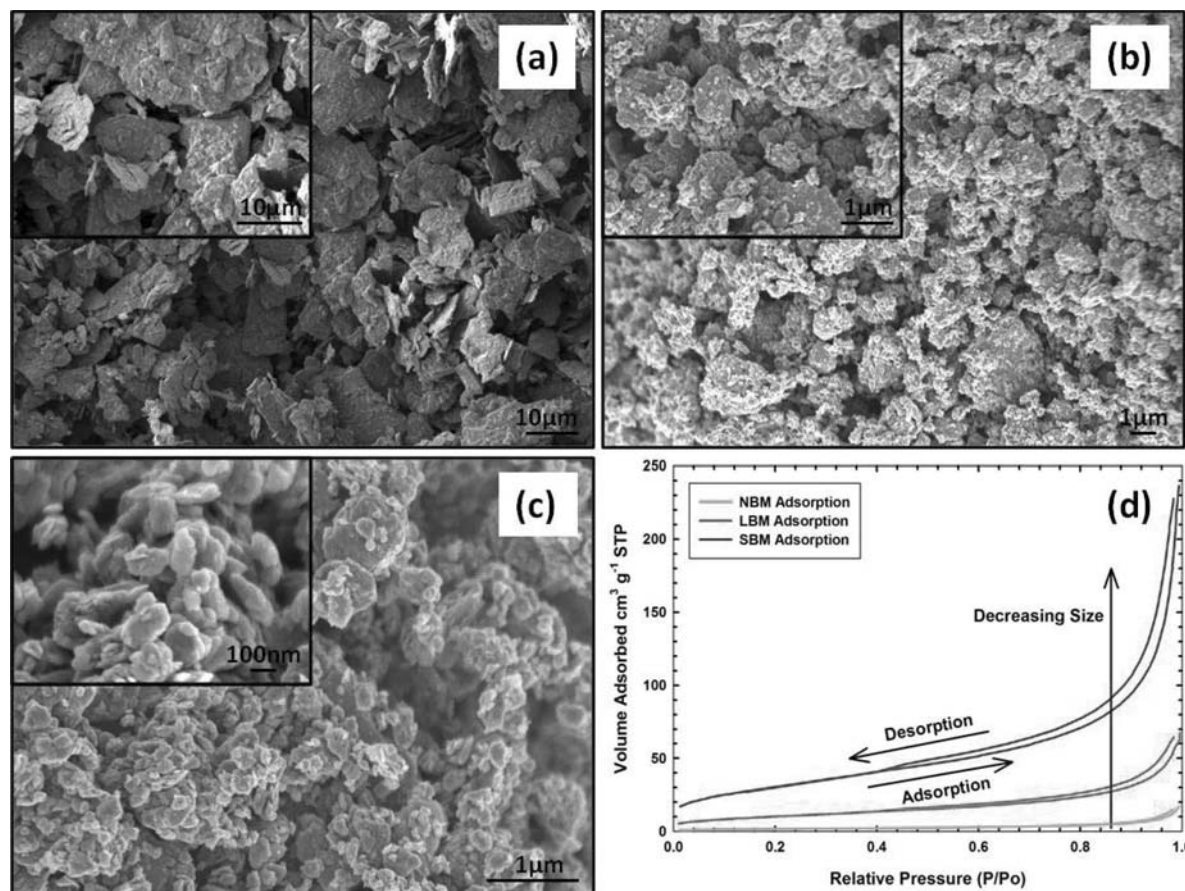


Figure 1. FESEM micrographs of (a) NBM, (b) LBM, and (c) SBM particles, showing a reduction in particle size of two orders of magnitude from NBM to SBM. (d) BET isotherms for NBM, LBM, and SBM showing significant increase in adsorption for size reduced materials.

approximately 10 μm . The layered structure of TiS_2 is very obvious among the NBM plate-like particles, of which layers we found to be approximately 100 nm thick through further imaging. We fabricated two sizes of ball-milled material using different size balls, large and small. The material produced with the large balls is referred to as large-ball-milled TiS_2 (LBM) and the material produced with smaller balls is referred to as small-ball-milled TiS_2 (SBM). The FESEM imaging reveals that LBM has an average particle size near 1 μm , and the SBM to have a particle size of approximately 100 nm. However agglomeration of the SBM is observed as a result of the high surface energy of nanoparticles. We were able to successfully reduce the particle size of TiS_2 by two orders of magnitude to an average size of 100 nm by ball milling.

In order to confirm particle size and distribution of our materials we measured the specific surface area using Brunauer-Emmett-Teller (BET) adsorption. Figure 1d shows the isotherms collected for all three sizes of materials. The BET method involves the determination of the amount of the adsorbate or adsorptive gas required to cover the external and the accessible internal pore surfaces of a solid with a complete monolayer of adsorbate. This monolayer capacity can be calculated from the adsorption isotherm. For NBM we obtain a specific surface area of 5.63 $\text{m}^2 \text{g}^{-1}$ and for the LBM and SBM, 36.44 and 107.12 $\text{m}^2 \text{g}^{-1}$ respectively. These values confirm that we are effectively increasing the surface area of particles by reducing their size. A non-linear trend of increasing specific surface area is observed for particles due to the change in overall shape of particles with size reduction, as shown in Figure 1. As we reduce the particle size to the nanoscale, we see more cylinder-like than plate-like particles. Broad size distribution, agglomeration, and changing particle geometry attribute to inconsistencies between the FESEM estimated particle sizes

and corresponding BET specific surface area, however there is good agreement in the overall trend between the two sets of data.

While ball milling is a proven technique for reducing particle size of materials, the process is also capable of changing the structure of materials.³⁶ To verify we have not changed the local structure of TiS_2 in reducing particle size, we show the Raman spectra for all three materials in Figure 2a. We see no significant changes in structure as the characteristic frequencies for all materials are consistent. Raman spectra of our TiS_2 show strong scattering at 334 cm^{-1} with a shoulder at 380 cm^{-1} and a very shallow scattering peak in the region of 227 cm^{-1} , which agrees well with previous literature.^{37–39} To further verify the structure of our size reduced materials, we show x-ray diffraction (XRD) patterns for all materials in Figure 2b. Collected data is consistent with HCP 1T- TiS_2 powder reported in the previous literature.^{40–42} The NBM exhibits all of the signature peaks of TiS_2 with good relative intensity while the LBM and SBM resulted in intensity reduction and/or complete vanishing of the (00l) planes (basal plane) peaks. This result is consistent with the FESEM micrographs in Figure 1 through observation of the plate-like structure of NBM and the more cylinder-like particles of LBM and SBM. Because we have eliminated the very long range order of the micrometer-sized layered particles we observe a marked decrease of intensity for respective peaks. We also observe the overall reduction of peak intensity as a result of reduced grain size and/or reduced crystallinity.⁴³ Raman spectroscopy and XRD measurements confirm that TiS_2 powder maintains structural stability as particle size is reduced by high energy ball-milling.

Electrochemical Measurements and Analyses.— In order to examine the capabilities of the composites when used as cathode materials

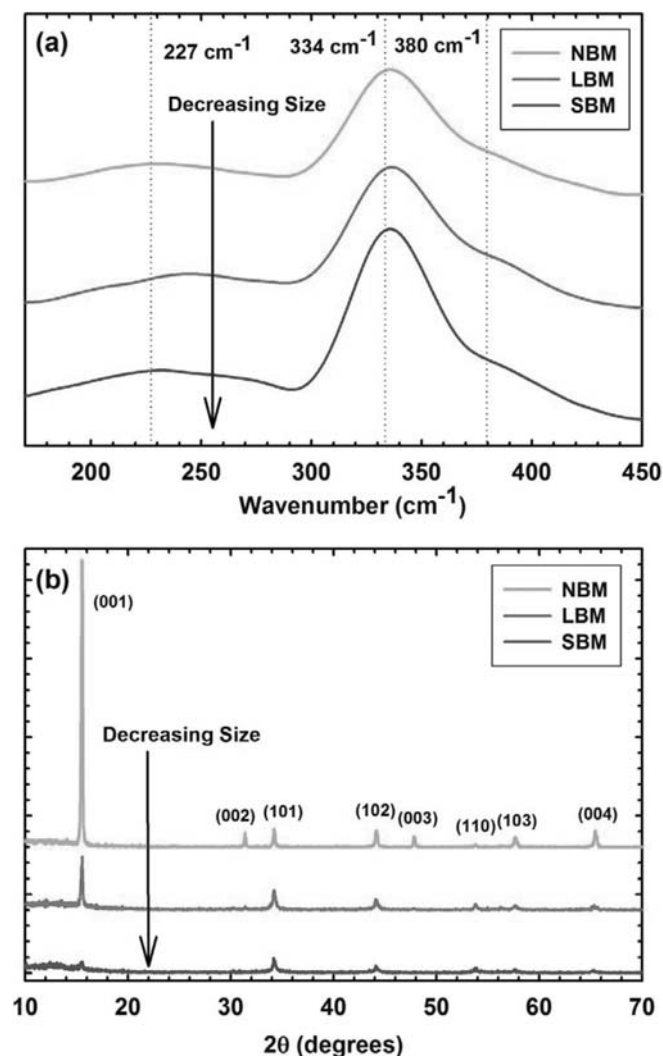


Figure 2. (a) Raman spectra for NBM, LBM, and SBM show no significant change in microstructure as particle size decreases. (b) X-ray diffraction patterns for all three TiS_2 materials revealing no significant structural changes related to ball milling of TiS_2 to reduce particle size. Basal plane indexes fade as particle size is reduced and the structure of TiS_2 is changed from plate-like to cylinder-like.

for rechargeable batteries, composite/solid-electrolyte/lithium cells were fabricated and characterized. Initial efforts focused on determination of an ideal cathode composite construction regarding the ratio of active material to solid electrolyte. Based upon observation of highest obtainable capacity, cycle life, and coulombic efficiency at relatively low rates and at room temperature, we determined an ideal ratio of 1:2 of active material and solid electrolyte respectively, for constructing our composite cathodes. Incorporation of a conductive additive (acetylene black) at the various tested composite compositions showed insignificant changes regarding capacity, cycle life, and efficiency and confirmed best results using a ratio of 1:2 for active material and solid electrolyte respectively.

After determination of ideal composite construction, battery characterization was focused on achieving high power density from our cathode. Figure 3a shows the rate performance of NBM at room temperature with and without a conductive additive. We see a comparison of the typical discharge profiles for both samples showing little difference in performance at low rates. This result indicates that no conductive additive is necessary for use with a TiS_2 based electrode due to its mixed conducting properties. In particular electronically conducting properties are high enough to sustain fast electron trans-

port through the composite to the current collector.^{25,30} Furthermore, we find that at high rate, incorporation of a conductive additive into the composite cathode actually decreases performance significantly. When cycled at a rate of 5 C, a 23% decrease in achievable capacity has been observed for batteries with an addition of only ~3% acetylene black. Further addition of acetylene black showed a continued trend of decreasing cell performance. Testing with ball-milled materials as well as testing at elevated temperatures yielded similar results, with an overall observation of decreased performance with the addition of conductive additive to composite cathodes at high rates. This drop in high rate performance is attributed to the conductive additive blocking of ion conduction from the active material TiS_2 particles. As we depict in Figure 3b the acetylene black is essentially acting as an ionically insulating layer around the active material particles, effectively limiting the capacity at high rates. At low rates, this barrier effect is not observed because the transport capabilities of TiS_2 are beyond what is required for the applied current. TiS_2 maintains a high electrical conductivity in solid state composite cathodes and is sufficient enough for electron transport without the use of a conductive additive.

In order to examine the practical power density capabilities of the composites when used as cathode materials for rechargeable batteries, the composite/solid-electrolyte/lithium cells were discharged at various current rates ranging from .2 C up to 10 C with a charging rate of 0.5 C. Figure 4a shows the voltage discharge profiles from electrochemical testing of all three sizes of material at room temperature with increasing rates. We observe significantly better results from ball-milled materials over the NBM material, with only slight variation in performance between the ball-milled samples. We attribute the increased capacity of ball-milled materials at high rates to the reduced particle size of TiS_2 . Smaller particles have shorter lithium diffusion paths and better kinetic properties that allow for better utilization of active materials.^{44,45} We observe only slight variation of performance between the ball-milled samples which is attributed to the limited ionic conductivity of the solid electrolyte at room temperature. Due to a relatively low bulk conductivity of the solid electrolyte at room temperature, observation of the kinetic benefit associated with reduced particle size is difficult to recognize. As the conductivity of the electrolyte is limiting at room temperature, we tested batteries at 60°C under the same conditions as the room temperature cells, which is reported in Figure 4b. At elevated temperature, the ionic conductivity of the solid electrolyte is no longer limiting and we can clearly observe a difference in kinetic behavior with changing material size. One obvious effect is the high rate capability at elevated temperature. For room temperature samples we observe an appreciable capacity up to only 6 C, whereas at elevated temperature we successfully cycle at 10 C. We observe a marked enhancement of high rate performance from cells at elevated temperature, especially for the SBM material. The SBM material exhibits a discharge capacity of 180 mAh g⁻¹ at 10 C when cycling at elevated temperature. It shows no loss in capacity ranging from 0.2 C up to 2 C, maintaining almost theoretical capacity for TiS_2 at 239 mAh g⁻¹. Increasing the applied current from 0.2 C up to 10 C for all materials at elevated temperature we see a 92% decrease in capacity for NBM composites and 86% decrease for LBM composites, but observe only a 25% decrease in achievable capacity for SBM materials. We attribute this excellent capacity retention to the reduced size of particles. The size reduced particles allow for improved Li ion kinetics resulting in a more effective utilization of active material.

A synopsis of the power capabilities of the different materials at both room and elevated temperature is shown in Figure 5. The Ragone plot shows the relationship between the energy density and the average power density of cells cycled at various current densities. We see that high temperature samples show an excellent improvement in power over room temperature samples, with SBM material exhibiting over 1000 W kg⁻¹ at 10 C. In comparison to current state-of-the-art (SOA) power density of liquid cells, we see that the power density of our SBM material at 60°C is beyond the current state-of-the-art capabilities.²⁰ Typical commercial liquid batteries employing LiCoO_2 are not safe

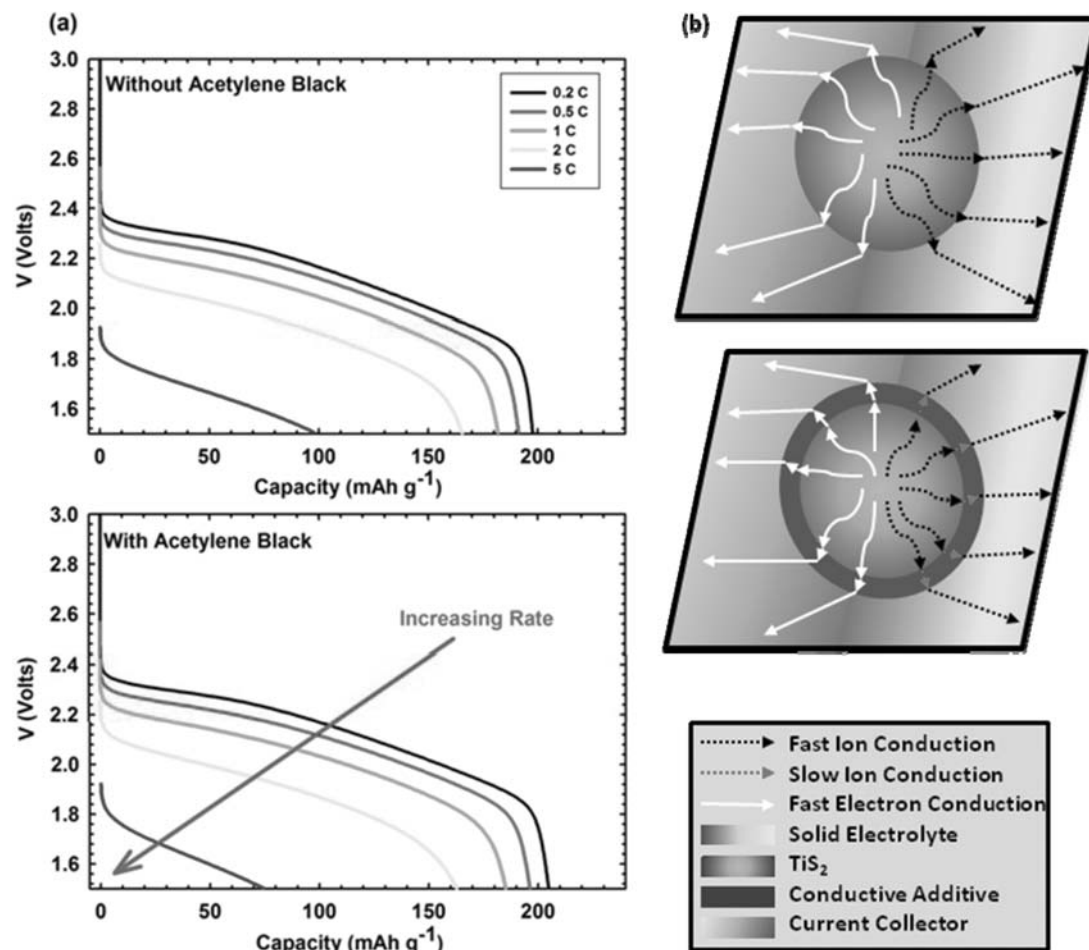


Figure 3. (a) Effect of conducting additive (AB) on the electrochemical rate capability of TiS₂ composite electrodes. The horizontal axis indicates the specific capacity that was calculated on the basis of the weight of the active material. (b) Mechanistic diagram of slowed ion conduction as a result of conductive additive blocking. Fast electron conduction is maintained through the AB but mass transfer is restricted as a result of poor ion conducting properties.

for operation at elevated temperature due to potential overcharge and heightened probability of a thermal reaction.

We used the galvanostatic intermittent titration technique (GITT) as a means of evaluating the increased effective surface area within composite electrodes resulting from reduced particle size. This technique as described by Weppner and Huggins combines both transient and steady-state measurements to obtain kinetic properties of solid mixed-conducting electrodes.⁴⁶ Generally, the physical quantities of a material and electrochemical measurements can be used to calculate the chemical diffusion coefficient of a material. However, calculation of the diffusion coefficient requires knowledge of the effective surface area of your electrode material, which is a considerably difficult value to measure for a composite mixture. Assuming a constant chemical diffusion coefficient in the range of $x = 0.50$ in Li_{*x*}TiS₂ for our structurally consistent materials we compute the effective surface area of our electrodes to show increased surface area for size reduced TiS₂ electrodes, thereby confirming enhanced kinetic properties corresponding to smaller particles.⁴⁷ The equation for the calculating the surface area *S* (cm²) was derived by Weppner and Huggins:

$$D_{Li} = \left(\frac{V_M}{S F} \right)^2 \times \left[I^0 \left(\frac{\delta E / \delta x}{\delta E / \delta t^{1/2}} \right) \right]^2 \text{ at } t \ll \tau \quad [1]$$

where D_{Li} is the chemical diffusion coefficient (1×10^{-9} cm² s⁻¹),³¹ V_M is the molar volume (36.11 cm³ mol⁻¹), *S* is the effective contact area between electrolyte and active material, *F* is the Faraday constant (96486 C mol⁻¹), I^0 is the applied constant electric current (4.0×10^{-4} A), $\delta E / \delta x$ is the slope of the coulometric titration curve,

and $\delta E / \delta t^{1/2}$ is the slope of the short time transient voltage change for a material.

The coulometric titration (CT) curves for both room temperature and elevated temperature samples can be seen in Figure 6a, which represent the evolution of the equilibrium potential vs. *x* in Li_{*x*}TiS₂. Cells were discharged at a rate of *C*/2 and allowed to rest for 2 hours before recording the open circuit potential. Assuming the complete reaction:



we observe the slopes for all samples at Li_{0.5}TiS₂ are similar.³³ The point Li_{0.5}TiS₂ is used for calculation because the voltage is relatively constant over a large concentration of *x*, whereas at Li_{1.0}TiS₂ the voltage changes dramatically and is therefore not a suitable point for estimation. An increasing voltage for Li_{1.0}TiS₂ at elevated temperature for the different materials indicates the better utilization of active material. As the size of particles is reduced, the relaxation time and potential difference between dynamic and equilibrium curves decreases, which agrees with the reduced time constant of particles exhibiting shorter diffusion paths. Figure 6b shows the transient voltage slopes for all samples collected from the galvanostatic pulse as a function of the square root of the time for Li_{0.5}TiS₂. No difference is observed for room temperature samples; however a large difference in slope for the elevated temperature samples is apparent. As previously discussed, the effects of relatively low ionic conductivity of solid electrolyte dominate kinetics at room temperature invalidating the equation developed by Weppner and Huggins. At high temperature

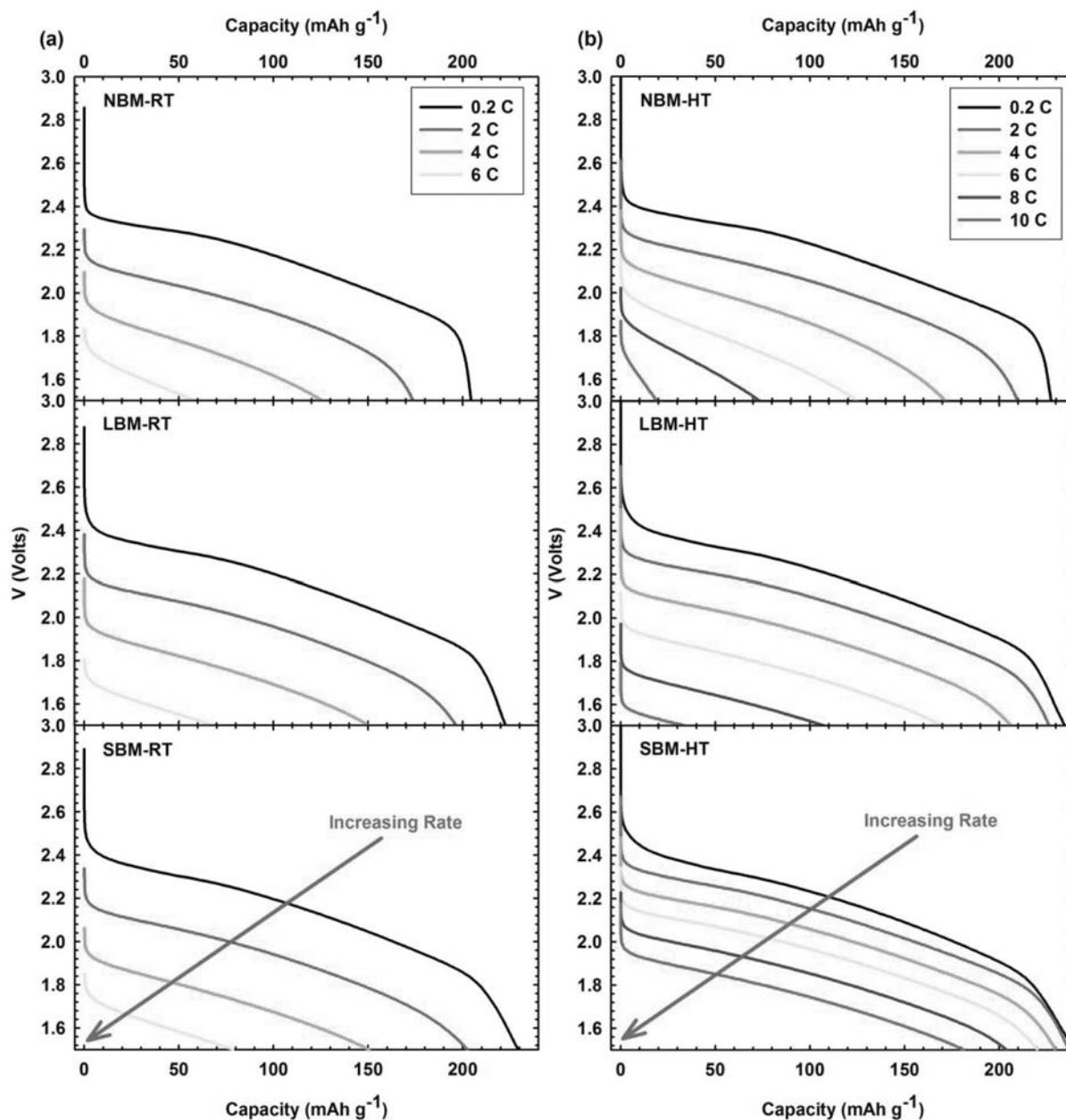


Figure 4. Electrochemical rate testing of all three materials at (a) room temperature and (b) elevated temperature showing superior rate performance of SBM. The notation (-RT) indicates samples tested at approximately room temperature 25°C, while the notation (-HT) denotes samples tested at high (elevated) temperature tested at approximately 60°C. Room temperature rate testing succeeded at current densities up to 6 C while the rate testing of elevated temperature samples succeeded at current densities up to 10 C.

however, we observe a very significant change in slope, verifying a trend of faster kinetics of the size reduced materials. Using the slope of the transient-voltage GITT curves and the slope of the equilibrium-voltage CT curves in Table I we calculate the active surface area of the composite electrodes. The effective surface area of LBM is 152%

Table I. Electrode surface area for elevated temperatures.

	NBM	LBM	SBM
CT Slope ($-V \delta x^{-1}$)	7.71×10^{-1}	7.65×10^{-1}	7.47×10^{-1}
GITT Slope ($-V s^{-1/2}$)	2.66×10^{-1}	1.70×10^{-1}	1.07×10^{-1}
Surface Area (cm^2)	1.78	2.71	5.31

higher than the area of NBM while the increase in area from NBM to SBM is an astonishing 298%. We have confirmed an increased contact surface area up to 300% for the size reduced materials and shown that relatively low bulk solid electrolyte conductivity at room temperature prevents the accurate measurement of kinetic benefits resulting from size reduction.

As stated, solid electrolyte effects dominate at room temperature which prevents measurement of kinetic properties, invalidating the equation proposed by Weppner and Huggins for calculation of the chemical diffusion coefficient. Using electrochemical impedance spectroscopy (EIS) we show that only resistance for the bulk solid electrolyte layer is obtainable at room temperature in Figure 7. No appreciable difference for decreasing interfacial resistance with smaller active material particles is observed as a result of the large solid electrolyte resistance effects at room temperature. At elevated

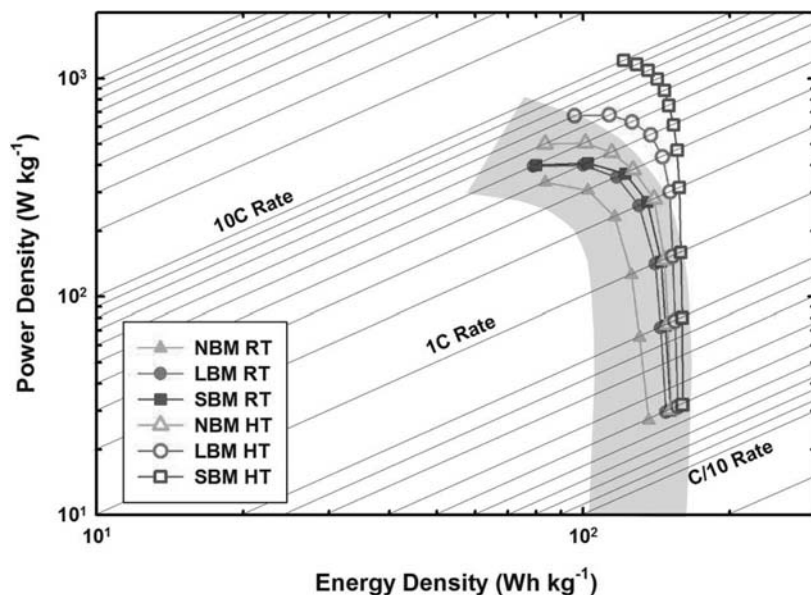


Figure 5. Ragone plot summarizing the power/energy density of TiS_2 materials vs. the state-of-the-art Li-ion technology. The plots for the present battery are based on weight of cathode composite only and derived from the discharge curves in Figure 4. The shaded area indicates the energy and power densities of commercialized lithium-ion batteries reported in literature.¹⁴

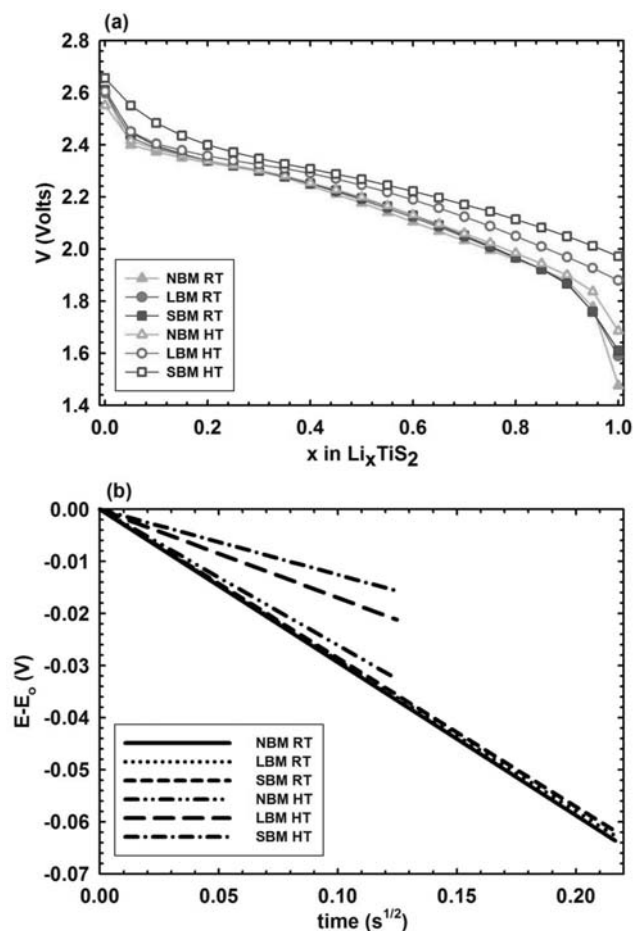


Figure 6. (a) Quasi-equilibrium potential vs. Li in Li_xTiS_2 as a function of stoichiometry x for both room temperature (RT) and elevated temperature (HT) samples. While potentials vary for different materials and temperatures, very similar slopes are observed for all samples in the region of $x = 0.50$. (b) Representation of the transient voltage of the GITT pulse as a function of square root of time for $\text{Li}_{0.5}\text{TiS}_2$ for all room temperature and elevated temperature samples. A significant change in slope is observed for elevated temperature samples while no change is observed for room temperatures samples.

temperature however, we see a clear distinction between the interfacial resistances for the various sizes of materials with a 250% increase in ionic conductivity from $1 \times 10^{-3} \text{ S cm}^{-1}$ to $2.5 \times 10^{-3} \text{ S cm}^{-1}$ for room to elevated temperature respectively. While extrapolation of the actual interfacial resistance cannot be made, it is clear from the magnitude of resistance corresponding to the various sizes of materials in Figure 7 that a significantly lower interfacial resistance exists.

In order to show the high rate cycle life of TiS_2 in solid state we cycled the composite/solid-electrolyte/lithium batteries with a discharge rate of 2 C and a charge rate of 0.5 C. The first cycle of cells was discharged and charged at a rate of 0.2 C. Figure 8a and 8b show the room temperature and elevated temperature high rate cycle life for all three sizes of materials respectively. We observe an average reversible capacity over 90% of the initial capacity after 50 cycles for all samples. There is an approximate 20% increase in capacity for ball-milled materials at room temperature, with an additional 15%

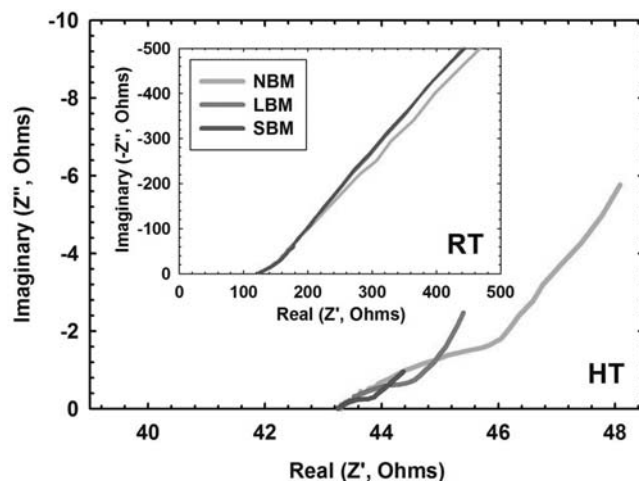


Figure 7. Electrochemical impedance spectroscopy measurements for both room temperature and high temperature batteries at $\text{Li}_{0.5}\text{TiS}_2$. Room temperature testing exhibits no change in kinetics as a result of increased surface area, whereas high temperature testing reveals the enhanced interfacial kinetics. The bulk conductivity for all samples is the same while we see a marked difference in interfacial resistance between the NBM, LBM, and SBM samples.

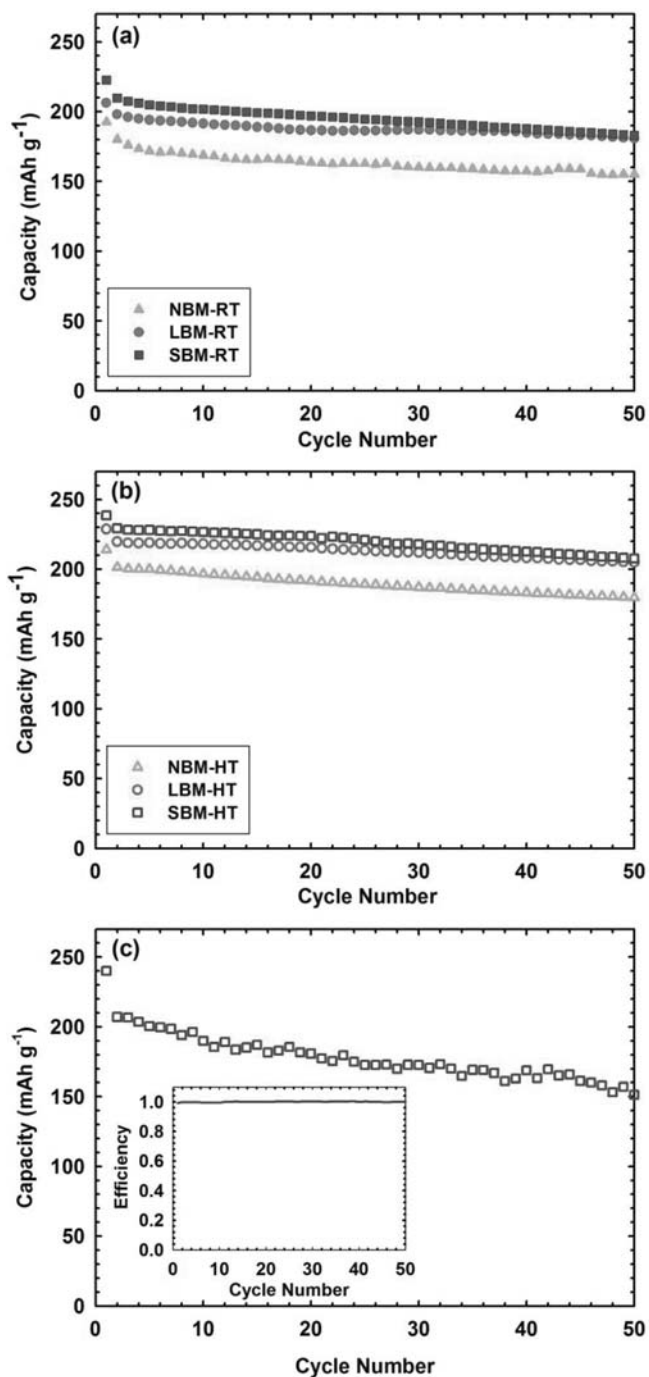


Figure 8. Reversible capacity increases for reduced particle size for both (a) room temperature and (b) elevated temperature cycling at 2 C-rate, and (c) SBM at 10 C-rate showing that the size reduced TiS₂ composite is capable of maintaining a high power density over 1000 W kg⁻¹ for over 50 cycles.

increase in reversible capacity for the relative elevated temperature samples. The increase in capacity at room temperature is a result of smaller size and better utilization of materials. The increase in capacity for samples at high temperature is a result of increased surface area and utilization, as well as improved kinetics that result in a higher reversible capacity. The SBM material exhibits a theoretical capacity of 239 mAh g⁻¹ assuming a complete reaction $\text{TiS}_2 + \text{Li} \rightarrow \text{Li}_1\text{TiS}_2$. In general, testing at elevated temperatures results in more pronounced undesired side reactions between the electrode material and the solid electrolyte. In the case of TiS₂ however, we observe negligible degra-

ation for material tested at elevated temperature vs. testing at room temperature. This speaks highly to the stability of TiS₂ in a solid state configuration with a sulfide electrolyte as this suggests no increased reactions in the electrode as a result of an elevated temperature environment.

With the intention of demonstrating TiS₂ as a long lasting and high power electrode material for solid state batteries that can outperform current state-of-the-art batteries, we applied a rigorous testing procedure with a discharge rate of 10 C to observe cycle life at extremely high rate. Again, using a first cycle discharge/charge rate of 0.2 C and a continued cycling charge rate of 0.5 C we observe the cycle life of the best performing material, SBM TiS₂. Figure 8c shows the cycling behavior of the SBM cell cycled at elevated temperature. We see an initial capacity of the 2nd cycle at 208 mAh g⁻¹ and maintain a capacity over 150 mAh g⁻¹ for 50 cycles. This translates to an initial power density of almost 1400 W kg⁻¹ and a maintained power density over 1000 W kg⁻¹ for 50 cycles. This high rate cycling result is noteworthy because typically high rate cycling in solid-state results in fast capacity fade and low overall capacity. We see a high first cycle efficiency over 97% and continued cycling at almost unity. We do observe some minor capacity losses as a result of extremely high rate cycling. We achieved a maximum power density of the composite over 1400 W kg⁻¹ and maintained over 1000 W kg⁻¹ for 50 cycles at a rate of 10 C.

Conclusions

Durable and extremely high power rechargeable all-solid-state Li batteries are constructed using TiS₂ nanocomposites. Particle size of TiS₂ is reduced by high energy ball-milling and enhanced performance of nanocomposite cathodes in solid-state Li batteries is observed. The better utilization of active material and fast kinetics resulting from the size reduction of TiS₂ allows for highly reversible capacity in both room temperature and elevated temperature environments. Nanocomposite electrodes with better overall kinetics can be constructed without a conductive additive as the use of acetylene black is shown to degrade performance at high rate. Average capacity fade for all cells is less than 10% over 50 cycles while excellent reversible capacity for room temperature batteries and near theoretical capacity for elevated temperature batteries was observed. High power all-solid-state batteries were constructed with nano-sized TiS₂ and demonstrated high power density over 1000 W kg⁻¹ for over 50 cycles, with a maximum power density of almost 1400 W kg⁻¹.

The drawback to using TiS₂ as an electrode material is the relatively low voltage compared to conventional lithium-ion batteries. However, with further optimization of electrode composites and manufacturing methods, these batteries could find potential for automotive applications in elevated temperature environments. Further developments with TiS₂ electrodes should focus on increasing the energy density.

Experimental

Preparation of the TiS₂ active materials.— TiS₂ (Sigma-Aldrich, 99.9%) was ball milled in a 100 mL agate vial (Across International) at a net weight of 500 mg. Large-ball-milled (LBM) material was prepared using 10 agate balls (10 mm diameter) and small-ball-milled (SBM) material with 50 agate balls (6 mm diameter) for grinding. Ball milling (Across International PQ-N4) took place for 2 continuous hours for LBM material and 5 continuous hours for SBM material in an Argon environment before the material was recovered and used without further modification.

Preparation of the Solid-State Electrolyte TiS₂ Composite Cell.— 77.5Li₂S-22.5P₂S₅ (mol%) electrolyte prepared by planetary ball milling in a ratio of was used as the solid-electrolyte (SE).³⁵ Milling resulted in amorphous electrolytes with room temperature and elevated temperature conductivity of 9.3×10^{-4} S cm⁻¹ and 2.5×10^{-3} S cm⁻¹ respectively. Composite electrodes were prepared

by mixing our ball milled and non-ball-milled TiS₂ powders with SE in a mortar at a ratio of 1:2 respectively. For composites including acetylene black (AB) (Alfa-Aesar, 50% compressed) as a conductive additive, a ratio of 10:20:1 was used for the TiS₂, solid electrolyte, and acetylene black respectively. Battery pellets are formed by cold-pressing (5 metric tons) 10 mg of the composite cathode material on top of 200 mg of SE for 5 min. Li foil (Alfa-Aesar, 0.75 mm thick) is then attached to the SE surface at 2 metric tons. All pressing and testing operations are carried out in a polyaryletheretherketone (PEEK) mold ($\phi = 1.3$ cm) with Ti metal rods as current collectors for both working and counter electrodes. All processes were carried out in an Ar-filled glove box.

Cell Testing.—Galvanostatic constant-current-constant-voltage (CCCV) charge-discharge cycling took place between 1.5 and 3.0 V at room temperature (25°C) and high temperature (60°C) using an Arbin BT2000 with a one hour voltage hold at 3.0 V after constant current charging. The Galvanostatic Intermittent Titration Technique (GITT) used 0.5C discharging for both discharge of the cell, and pulse measurement. Rest time for GITT testing was 2 hours, and the pulse time was 30 seconds, with a 30 second rest after the pulse before resuming discharge. Ball milled powder samples were characterized by XRD Cu-K α radiation (Scintag XGEN-4000) measurement and Raman spectroscopy (Jasco NRS-3100).

Acknowledgment

The authors gratefully acknowledge support for this work from the DARPA Defense Sciences Office.

References

1. B. SCROSATI, *Nature*, **393**, 557 (1995).
2. G. Ceder, Y. Chiang, D. Sadoway, M. Aydinol, Y. Jang, and B. Huang, *Nature*, **392**, 694 (1998).
3. J. Wang, J. Yang, C. Wan, K. Du, J. Xie, and N. Xu, *Advanced Functional Materials*, **13**, 487 (2003).
4. M. Armand and J. Tarascon, *Nature*, **451**, 652 (2008).
5. Y.-G. Guo, J.-S. Hu, and L.-J. Wan, *Advanced Materials*, **20**, 2878 (2008).
6. B. Key, R. Bhattacharyya, M. Morcrette, V. Seznec, J. Tarascon, and C. Grey, *Journal of the American Chemical Society*, **131**, 9239 (2009).
7. D. Abraham, *Jom-Journal of the Minerals Metals & Materials Society*, **54**, 18 (2002).
8. S. Lee, N. Yabuuchi, B. Gallant, S. Chen, B. Kim, P. Hammond, and Y. Shao-Horn, *Nature Nanotechnology*, **5**, 531 (2010).
9. J. Tarascon and M. Armand, *Nature*, **414**, 359 (2001).
10. P. Bruce, *Solid State Ionics*, **179**, 752 (2008).
11. F. Mizuno, A. Hayashi, K. Tadanaga, T. Minami, and M. Tatsumisago, *Journal of Power Sources*, **124**, 170 (2003).
12. Y. Rho and K. Kanamura, *Journal of Power Sources*, **158**, 1436 (2006).
13. N. Machida, H. Maeda, H. Peng, and T. Shigematsu, *Journal of the Electrochemical Society*, **149**, A688 (2002).
14. Y. Jung, A. Cavanagh, A. Dillon, M. Groner, S. George, and S. Lee, *Journal of the Electrochemical Society*, **157**, A75 (2010).
15. M. Winter, J. Besenhard, M. Spahr, and P. Novak, *Advanced Materials*, **10**, 725 (1998).
16. A. Hayashi, S. Hama, T. Minami, and M. Tatsumisago, *Electrochemistry Communications*, **5**, 111 (2003).
17. P. Knauth, *Solid State Ionics*, **180**, 911 (2009).
18. K. Takada, N. Ohta, L. Zhang, K. Fukuda, I. Sakaguchi, R. Ma, M. Osada, and T. Sasaki, *Solid State Ionics*, **179**, 1333 (2008).
19. K. Minami, A. Hayashi, and M. Tatsumisago, *Solid State Ionics*, **179**, 1282 (2008).
20. N. Ohta, K. Takada, L. Zhang, R. Ma, M. Osada, and T. Sasaki, *Advanced Materials*, **18**, 2226 (2006).
21. A. Sakuda, H. Kitaura, A. Hayashi, K. Tadanaga, and M. Tatsumisago, *Journal of Power Sources*, **189**, 527 (2009).
22. Y. Nishio, H. Kitaura, A. Hayashi, and M. Tatsumisago, *Journal of Power Sources*, **189**, 629 (2009).
23. H. Kitaura, A. Hayashi, T. Ohtomo, S. Hama, and M. Tatsumisago, *Journal of Materials Chemistry*, **21**, 118 (2011).
24. A. Patil, V. Patil, D. Shin, J. Choi, D. Paik, and S. Yoon, *Materials Research Bulletin*, **43**, 1913 (2008).
25. M. Whittingham, *Chemical Reviews*, **104**, 4271 (2004).
26. B. Ellis, K. Lee, and L. Nazar, *Chemistry of Materials*, **22**, 691 (2010).
27. K. Takada, T. Inada, A. Kajiyama, M. Kouguchi, H. Sasaki, S. Kondo, Y. Michiue, S. Nakano, M. Tabuchi, and M. Watanabe, *Solid State Ionics*, **172**, 25 (2004).
28. A. Sakuda, H. Kitaura, A. Hayashi, K. Tadanaga, and M. Tatsumisago, *Journal of the Electrochemical Society*, **156**, A27 (2009).
29. H. Kitaura, A. Hayashi, K. Tadanaga, and M. Tatsumisago, *Journal of the Electrochemical Society*, **157**, A407 (2010).
30. M. Whittingham, *Progress in Solid State Chemistry*, **12**, 41 (1978).
31. A. Vaccaro, T. Palanisamy, R. Kerr, and J. Maloy, *Solid State Ionics*, **2**, 337 (1981).
32. R. Winter and P. Heitjans, *Journal of Physical Chemistry B*, **105**, 6108 (2001).
33. M. Whittingham, *Science*, **192**, 1126 (1976).
34. J. Kano, H. Yamashita, and F. Saito, *Powder Technology*, **98**, 279 (1998).
35. J. Trevey, J. S. Jang, Y. S. Jung, C. R. Stoldt, and S. H. Lee, *Electrochemistry Communications*, **11**, 1830 (2009).
36. K. MacKenzie, S. Komphanchai, and R. Vagana, *Journal of the European Ceramic Society*, **8**, 177 (2008).
37. C. Carmalt, S. O'Neill, I. Parkin, and E. Peters, *Journal of Materials Chemistry*, **14**, 830 (2004).
38. C. Carmalt, I. Parkin, and E. Peters, *Polyhedron*, **22**, 1263 (2003).
39. C. Carmalt, C. Dinnage, and I. Parkin, *Journal of Materials Chemistry*, **10**, 2823 (2000).
40. D. Li, X. Qin, and Y. Gu, *Materials Research Bulletin*, **41**, 282 (2006).
41. V. Pore, M. Ritala, and M. Leskela, *Chemical Vapor Deposition*, **13**, 163 (2007).
42. A. L. Let, D. E. Mainwaring, C. Rix, and P. Murugaraj, *Journal of Non-Crystalline Solids*, **354**, 1801 (2008).
43. G. Rieck and K. Koopmans, *British Journal of Applied Physics*, **3**, 419 (1964).
44. J. Wang, J. Yang, J. Xie, and N. Xu, *Advanced Materials*, **14**, 963 (2002).
45. M. Wagemaker, F. Mulder, and A. Van der Ven, *Advanced Materials*, **21**, 2703 (2009).
46. W. Weppner, and R. Huggins, *Journal of the Electrochemical Society*, **124**, 1569 (1977).
47. T. Yamamoto, S. Kikkawa, and M. Koizumi, *Solid State Ionics*, **17**, 63 (1985).